

Article

# Reduced Bipolar Conduction in Bandgap-Engineered $n$ -Type $\text{Cu}_{0.008}\text{Bi}_2(\text{Te},\text{Se})_3$ by Sulfur Doping

Weon Ho Shin <sup>1,†</sup> , Hyun-Sik Kim <sup>2,†</sup>, Se Yun Kim <sup>3</sup>, Sung-sil Choo <sup>4</sup>, Seok-won Hong <sup>4</sup>, Yeseong Oh <sup>4</sup>, Yerim Yang <sup>4</sup>, Yoona Kim <sup>4</sup>, Hee Jung Park <sup>5</sup> and Sang-il Kim <sup>4,\*</sup>

<sup>1</sup> Department of Electronic Materials Engineering, Kwangwoon University, Seoul 01897, Korea; weonho@kw.ac.kr

<sup>2</sup> Department of Materials Science and Engineering, Hongik University, Seoul 04066, Korea; hyunsik.kim@hongik.ac.kr

<sup>3</sup> Samsung Electronics, Suwon 16678, Korea; ksyvip@gmail.com

<sup>4</sup> Department of Materials Science and Engineering, University of Seoul, Seoul 02504, Korea; cntjdtlf111@uos.ac.kr (S.-s.C.); seokown4926@uos.ac.kr (S.-w.H.); asdf85205@uos.ac.kr (Y.O.); yyl0201@uos.ac.kr (Y.Y.); yoona0319@uos.ac.kr (Y.K.)

<sup>5</sup> Department of Materials Science and Engineering, Dankook University, Cheonan 31116, Korea; parkjang@dankook.ac.kr

\* Correspondence: sang1.kim@uos.ac.kr

† These authors equally contributed to this study.

Received: 24 December 2019; Accepted: 8 January 2020; Published: 10 January 2020



**Abstract:** Significant bipolar conduction of the carriers in  $\text{Bi}_2\text{Te}_3$ -based alloys occurs at high temperatures due to their narrow bandgaps. Therefore, at high temperatures, their Seebeck coefficients decrease, the bipolar thermal conductivities rapidly increase, and the thermoelectric figure of merit,  $zT$ , rapidly decreases. In this study, band modification of  $n$ -type  $\text{Cu}_{0.008}\text{Bi}_2(\text{Te},\text{Se})_3$  alloys by sulfur (S) doping, which could widen the bandgap, is investigated regarding carrier transport properties and bipolar thermal conductivity. The increase in bandgap by S doping is demonstrated by the Goldsmid–Sharp estimation. The bipolar conduction reduction is shown in the carrier transport characteristics and thermal conductivity. In addition, S doping induces an additional point-defect scattering of phonons, which decreases the lattice thermal conductivity. Thus, the total thermal conductivity of the S-doped sample is reduced. Despite the reduced power factor due to the unfavorable change in the conduction band,  $zT$  at high temperatures is increased by S doping with simultaneous reductions in bipolar and lattice thermal conductivity.

**Keywords:** thermoelectric; bipolar conduction; S doping; bandgap; point defect

## 1. Introduction

$\text{BiTe}$ -based alloys are thermoelectric materials widely used for room-temperature applications such as solid-state cooling. However, the broader use of  $\text{BiTe}$ -based alloys is limited by their low thermoelectric conversion performance [1,2]. The thermoelectric performance has often been evaluated by the dimensionless figure of merit—thermoelectric figure of merit ( $zT$ ) =  $\sigma S^2 T / \kappa_{\text{tot}}$ , where  $\sigma$  is the electrical conductivity,  $S$  is the Seebeck coefficient,  $\kappa_{\text{tot}}$  is the total thermal conductivity, and  $T$  is the absolute temperature. The maximum  $zT$  of  $\text{Bi}_2(\text{Te},\text{Se})_3$   $n$ -type alloys is below one, while different studies on  $(\text{Bi},\text{Sb})_2\text{Te}_3$   $p$ -type alloys have demonstrated values higher than one. Recently, the  $zT$  of polycrystalline  $\text{Bi}_2(\text{Te},\text{Se})_3$   $n$ -type alloys has been improved by doping with the Cu element [3], but it is still lower than the  $p$ -type alloys. Considering the fact that the efficiency of a thermoelectric module is closely related to the average material  $zT$  between  $p$ - and  $n$ -type thermoelectric materials, the  $zT$  of  $p$ - and  $n$ -type alloys needs to be high and similar.

Many efforts have been made to increase the  $zT$  of both  $p$ - and  $n$ -type alloys. For  $(\text{Bi,Sb})_2\text{Te}_3$   $p$ -type alloys, substituting cation sites with Pb, Ag, and Cu elements has been effective in shifting the maximum  $zT$  to temperatures greater than 400 K [4]. The formation of 0-dimensional point defects (from substitutional doping) intensifies point-defect phonon scattering and suppresses lattice thermal conductivity. Point defects can also enhance the power factor ( $=S^2\sigma$ ) of the alloys by changing their band structures. A similar approach has also been adopted in  $\text{Bi}_2(\text{Te,Se})_3$   $n$ -type alloys by substituting the cation site with different elements. Unfortunately, the observed improvement in the power factor was negligible. This is due to a significant decrease in the  $S$  (compared to an increase in  $\sigma$ ) resulting from the increased carrier concentration from the doping. For the substitutional doping strategy to be successful in  $n$ -type alloys, additional band engineering, which improves the  $S$  by making the density-of-states effective mass ( $m^*$ ) greater near the Fermi level and/or opening up the bandgap (bipolar conduction suppression), is also required. The bipolar conduction of carriers in BiTe-based alloys with narrow bandgaps ( $E_g$ , 0.1–0.2 eV) becomes significant at higher temperatures [5–7], which leads to detrimental influences on the thermoelectric properties. The  $S$  rapidly decreases, while the bipolar thermal conductivity,  $\kappa_{bp}$ , rapidly increases at temperatures higher than 300 K. Therefore, the  $zT$  rapidly decreases at higher temperatures. The proper band modification with  $E_g$  widening is beneficial owing to the reduction in detrimental influence, including the rapid  $S$  decrease and the  $\kappa_{bp}$  increase. In  $p$ -type  $(\text{Bi,Sb})_2\text{Te}_3$ , the  $E_g$  widening by In doping increases the  $zT$  by reducing  $\kappa_{bp}$ , while simultaneously reducing the lattice thermal conductivity,  $\kappa_{latt}$ , owing to the additional point defects originated from the doping [8].

The crystal structure of  $\text{Bi}_2\text{S}_3$  (orthorhombic phase) is different from those of  $\text{Bi}_2\text{Se}_3$  and  $\text{Bi}_2\text{Te}_3$  (rhombohedral phase, thus also from that of  $\text{Bi}_2(\text{Te,Se})_3$ ). However, a small amount of S doping in a  $\text{Bi}_2(\text{Te,Se})_3$   $n$ -type alloy would maintain its original crystal structure and would modify its electronic structure [9]. Typically, the  $E_g$  values of the series of tellurides, selenides, and sulfides with identical cations increase with the size of the anion [10–12]. Therefore, the  $E_g$  widening can be anticipated in S-doped  $\text{Bi}_2(\text{Te,Se})_3$  alloys. In this study, we investigated S-doped  $\text{Bi}_2(\text{Te,Se})_3$  alloys to evaluate the effects of S doping on the  $E_g$  and thermoelectric properties, while the Cu-doped  $\text{Bi}_2(\text{Te,Se})_3$  alloys were utilized due to their stability and higher  $zT$  than  $\text{Bi}_2(\text{Te,Se})_3$  alloys. A typical problem with  $\text{Bi}_2(\text{Te,Se})_3$   $n$ -type alloys is the lack of reproducibility of the thermoelectric properties, since Te vacancies are easily formed during synthesis [13]. Cu intercalation between the quintuple layer of Bi–Te material is known to suppress the formation of Te vacancies and improve reproducibility [14,15]. The thermoelectric properties of a series of S-doped  $\text{Cu}_{0.008}\text{Bi}_2\text{Te}_{2.8}\text{Se}_{0.2}$  ( $n$ -type  $\text{Cu}_{0.008}\text{Bi}_2\text{Te}_{2.8-x}\text{Se}_{0.2}\text{S}_x$ ,  $x = 0, 0.05, 0.15$ , and 0.30) samples were analyzed to verify the influence of S doping and  $E_g$  widening.

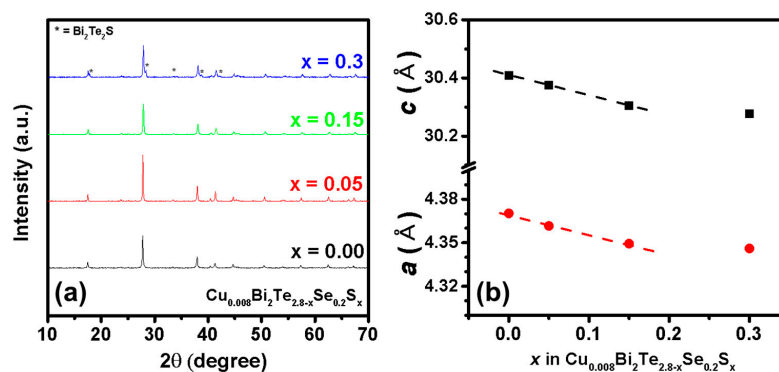
## 2. Materials and Methods

Bi (5N Plus, 99.999%), Te (5N Plus, 99.999%), Se (5N Plus, 99.999%), S (Sigma Aldrich, 99.999%), and Cu (Sigma Aldrich, 99.99%) were used as raw materials in the fabrication of the samples. Samples with compositions of  $\text{Cu}_{0.008}\text{Bi}_2\text{Te}_{2.8-x}\text{Se}_{0.2}\text{S}_x$  ( $x = 0, 0.05, 0.15$ , and 0.30) were synthesized by a solid-state reaction in a vacuum-sealed quartz tube (diameter: 15 mm) under  $10^{-5}$  Torr. The synthesized ingots were ball milled using a SPEX mill for 10 min. The sieved powders (below 45  $\mu\text{m}$ ) were spark plasma sintered at 723 K and 50 MPa for 2 min.

The crystallographic phases of the samples were determined by X-ray diffraction (XRD) with Cu  $K_{\alpha 1}$  ( $\lambda = 1.54059 \text{ \AA}$ ) radiation. The carrier concentrations were measured by Hall measurements in a magnetic field of 0.5 T (AHT-55T5, Ecopia, Toronto, ON, Canada) in the direction perpendicular to the pressing direction. The  $S$  and  $\sigma$  values in a temperature range of 320–520 K were measured using a thermoelectric property measurement system (ZEM-3) in a He atmosphere in the same direction. The  $\kappa_{tot}$  values were calculated using the sample densities ( $\rho_s$ ), heat capacities ( $C_p$ ), and thermal diffusivities ( $\lambda$ ) ( $\kappa = \rho_s C_p \lambda$ ). The temperature dependence of  $\lambda$  was measured using the laser flash method (LFA 457, Netzsch, Selb, Germany) in the same direction, so that the  $zT$  could be properly calculated.

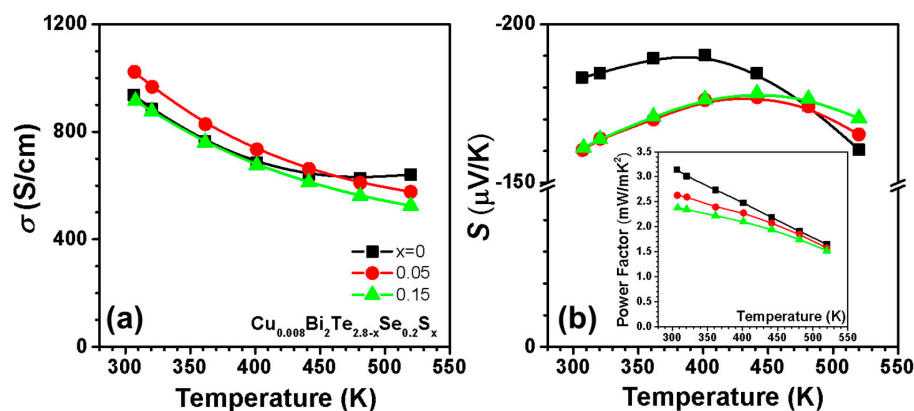
### 3. Results and Discussion

Figure 1a shows the XRD patterns of the investigated series of  $\text{Cu}_{0.008}\text{Bi}_2\text{Te}_{2.8-x}\text{Se}_{0.2}\text{S}_x$ , where  $x = 0, 0.05, 0.15$ , and  $0.30$ . The samples with  $x = 0, 0.05$ , and  $0.15$  exhibited single phases ( $\text{Bi}_2\text{Te}_{2.7}\text{Se}_{0.3}$ , JCPDS 00-050-0954) without impurities, while the highly doped sample with  $x = 0.3$  exhibited a phase separation with  $\text{Bi}_2\text{Te}_2\text{S}$  (JCPDS 00-042-1447). The calculated lattice parameters  $a$  and  $c$  (Figure 1b) simultaneously decreased with the S doping, as the S ion is considerably smaller than Te and Se. The systematic changes in  $a$  and  $c$  to  $x = 0.15$  imply that substitutional doping was successfully achieved. However, the observed phase separation with inconsistent changes in lattice parameters shows that the solid solution might be unstable near  $x = 0.3$ . Measurement of the thermoelectric transport properties was not carried out for  $x = 0.3$  (with a different phase).



**Figure 1.** (a) XRD patterns and (b) lattice parameters  $a$  and  $c$  of  $\text{Cu}_{0.008}\text{Bi}_2\text{Te}_{2.8-x}\text{Se}_{0.2}\text{S}_x$  ( $x = 0, 0.05, 0.15$ , and  $0.3$ ).

Figure 2a,b shows the  $\sigma$  and  $S$  values of the S-doped  $\text{Cu}_{0.008}\text{Bi}_2\text{Te}_{2.8-x}\text{Se}_{0.2}\text{S}_x$  ( $x = 0, 0.05$ , and  $0.15$ ) as functions of the temperature. The  $\sigma$  of the undoped sample was approximately 940 S/cm at 300 K, which slightly increased to 1020 S/cm for  $x = 0.05$ , and then decreased to 920 S/cm at  $x = 0.15$ . As shown in Figure 2b, the magnitude of the  $S$  at 300 K significantly decreased from 183 to  $\sim 160$   $\mu\text{V/K}$  by the doping. However, the undoped sample exhibited a decrease in the  $S$  at higher temperatures around 400 K, while the magnitudes of the  $S$  of the S-doped samples increased at temperatures higher than 440 K. At temperatures higher than 480 K, the magnitudes of the  $S$  of the S-doped samples were higher than those of the undoped sample. Thus, the power factor ( $S^2\sigma$ ) at 300 K (inset of Figure 2b) decreased with doping at all measurement temperatures.



**Figure 2.** (a) Measured electrical conductivities ( $\sigma$ ) and (b) Seebeck coefficients ( $S$ ) of  $\text{Cu}_{0.008}\text{Bi}_2\text{Te}_{2.8-x}\text{Se}_{0.2}\text{S}_x$  ( $x = 0, 0.05$ , and  $0.15$ ). The inset in (b) shows the temperature-dependent power factors of the samples.

According to the Goldsmid–Sharp equation [16], the  $E_g$  can be estimated as  $E_g = 2e|S_{max}|T_{max}$ , where  $T_{max}$  is the temperature at which the Seebeck coefficient has the maximum value. For the

S-doped sample, the  $E_g$  estimated by using the Goldsmid–Sharp equation was increased to 0.159 eV, compared to that of the undoped sample (0.152 eV) (Figure 3a). Figure 3b shows the  $S$  as a function of the carrier concentration,  $n$ , at 300 K. The effective mass ( $m_d^*$ ) was calculated using

$$S = \frac{8\pi^2 k_B^2}{3eh^2} \left( \frac{\pi}{3n} \right)^{2/3} m^* T \quad (1)$$

where  $k_B$ ,  $e$ ,  $h$ , and  $n$  denote the Boltzmann constant, elementary charge, Planck constant, and hole carrier concentration, respectively. The gray dashed lines correspond to  $m^* = 1.0$ , 1.1, and 1.2  $m_0$ , plotted using Equation (1). The  $m^*$  increased from 1.07 to 1.24 with the S doping to  $x = 0.15$ . This suggests that the conduction-band electronic structure of the  $n$ -type  $\text{Cu}_{0.008}\text{Bi}_2\text{Te}_{2.8}\text{Se}_{0.2}$  was modified by the S doping, along with possible bandgap modification. In other words, with increased S doping, the curvature of the conduction band was relaxed (the band became heavier), and its energy level was also increased relative to that of the valence band maximum.

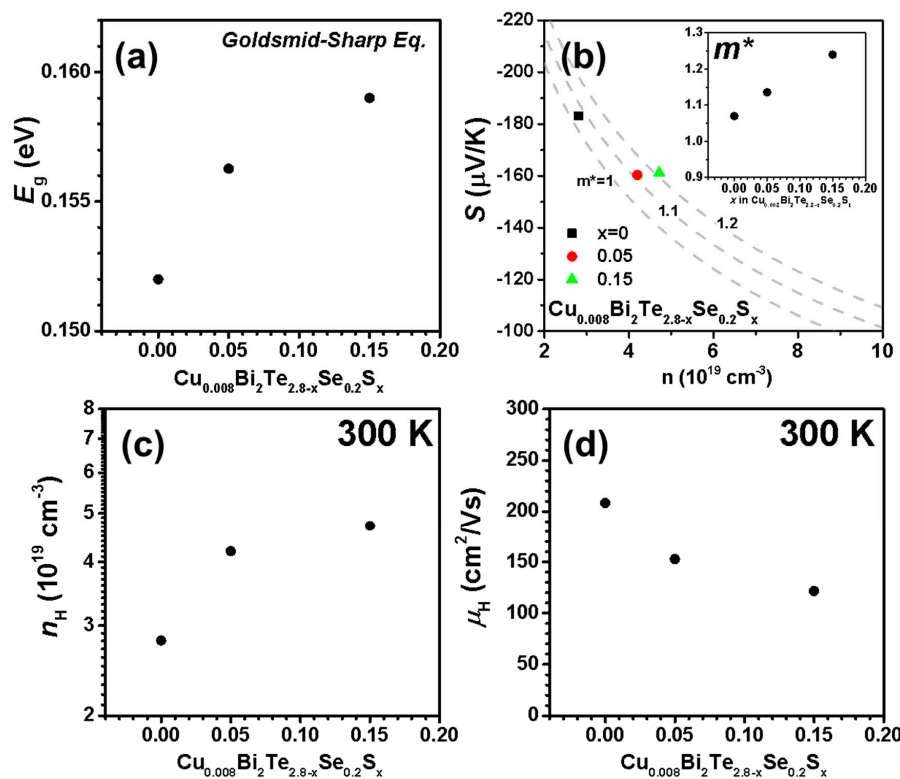


**Figure 3.** (a)  $E_g$  estimated using the Goldsmid–Sharp equation and (b) a Pisarenko plot. The inset shows the effective masses of the samples obtained using the Mott relationship. (c) Carrier concentrations  $n_H$  and (d) mobilities  $\mu_H$  estimated using the Hall measurement results.

The carrier concentrations ( $n$ ) and Hall mobilities ( $\mu_H$ ) estimated using the Hall measurement results are shown in Figure 3c,d. The  $n$  values at 300 K were  $2.8$ ,  $4.2$ , and  $4.7 \times 10^{19} \text{ cm}^{-3}$  at  $x = 0$ ,  $0.05$ , and  $0.15$ , respectively; they increased with the S doping. As the  $n$  is inversely proportional to the  $S$  according to Equation (1), the  $S$  with S doping observed in Figure 2b was lower than that without S doping, especially at temperatures lower than 450 K. However, at temperatures higher than 450 K, the  $S$  of the S-doped samples was higher than that of the pristine sample (without S doping). The overall  $S$  (when the majority carriers are electrons) measured in Figure 2b was in fact a conductivity-weighted average of the  $S$  from the conduction band ( $S_{CB}$ ) and the valence band ( $S_{VB}$ ),

as presented in Equation (2) below ( $\sigma_{CB}$  and  $\sigma_{VB}$  are the electrical conductivities from the conduction band and the valence band, respectively):

$$|S| = \frac{\sigma_{CB}|S_{CB}| - \sigma_{VB}|S_{VB}|}{\sigma_{CB} + \sigma_{VB}}. \quad (2)$$

For  $n$ -type materials, the carrier concentration of the holes present was much smaller than that of the electrons. As a result, the  $S_{VB}$  was much higher than the  $S_{CB}$  (based on Equation (1)), but as the  $\sigma_{VB}$  was negligible when compared to the  $\sigma_{CB}$  for the same reason, the contribution of the  $S_{VB}$  to the overall  $S$  was minimal at low temperatures. However, with increased temperature, the  $\sigma_{VB}$  was significantly improved owing to the broadening of the Fermi distribution. This was the reason behind the  $S$  rollover (due to bipolar contribution) observed in all the samples in Figure 2b. In addition, Figure 2b shows that the degrees of rollover for the S-doped samples were not as drastic as those measured for the pristine sample (without S doping). An enlarged bandgap with increased S doping (Figure 3a) is commonly known for suppressing the bipolar contribution to the overall  $S$  and to bipolar thermal conductivity. Therefore, the higher  $S$  of the S-doped samples in reference to that of the pristine sample originated from the enlarged bandgap. Notably,  $\mu_H$  at 300 K was significantly decreased to 121 at  $x = 0.15$ , compared to that of the undoped sample ( $208 \text{ cm}^2\text{V}^{-1}\text{s}^{-1}$ ). Therefore, the power factor was decreased (inset of Figure 2b), even with the  $m^*$  increase, which would imply that the conduction band was modified favorably for the  $S$ . The decrease should be related to both an increase in  $n$  and to possible impurity scattering by the S doping. The sudden increase in the electrical conductivity of  $x = 0.05$  (S doping) and its drop at higher S doping ( $x = 0.15$ ) can both be explained by an interplay between the decreasing  $\mu_H$  and increasing  $n$ .

To investigate the bipolar conduction of the samples, the characteristics of the hole carriers were deduced from the two-band model (conduction band (CB) and valence band (VB)) based on a single-parabolic-band model (Section S1 in Supplementary Materials) [17]. By using the measured  $\sigma$ ,  $S$ ,  $n$ , and  $\mu_H$  values, the deformation potentials ( $E_{def}$ ) and weighted mobilities ( $U$ ) for the CB and VB were calculated ( $U_{CB}$  and  $U_{VB}$ , respectively) (see Section S1 in Supplementary Materials) to investigate the carrier transport of electrons and holes, separately. The  $E_{def}$  describes the carrier–phonon interaction, e.g., a band with a large  $E_{def}$  has low mobility.  $U$ , the product of the nondegenerate mobility ( $\mu_0$ , as in Equation (1) as a function of  $E_{def}$ ) and  $(m^*)^{3/2}$  ( $U = \mu_0(m^*)^{3/2}$ ), elucidates the influence of the changes in the  $m^*$  and the  $E_{def}$  on the charge transport (Figure 4 and Table 1),

$$\mu_0 = \frac{e\pi\hbar^4 v_1^2 d}{\sqrt{2}E_{def}^2 m^{*5/2} (kT)^{3/2}}. \quad (3)$$

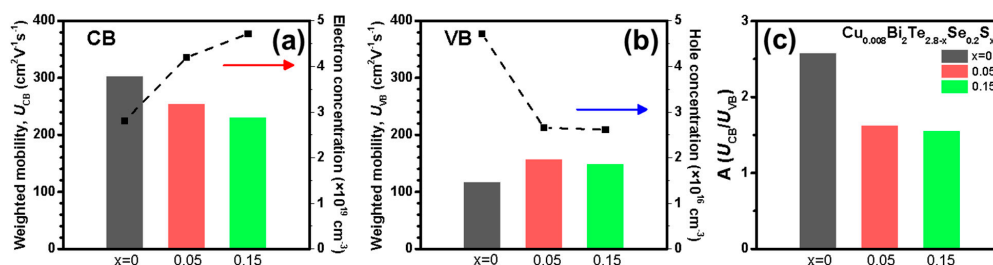


**Figure 4.** (a,b) Weighted mobilities for the conduction band (CB) and valence band (VB) of the measured samples, respectively. (c) Weighted mobility ratios of the  $\text{Cu}_{0.008}\text{Bi}_2\text{Te}_{2.8-x}\text{Se}_{0.2}\text{S}_x$  samples.

The  $U_{CB}$  decreased from 302 to  $230 \text{ cm}^2\text{V}^{-1}\text{s}^{-1}$ , while the  $U_{VB}$  increased from 117 to  $148 \text{ cm}^2\text{V}^{-1}\text{s}^{-1}$  upon S doping. Therefore, the S doping was detrimental to the electron carrier transport through the reduction in electron mobility,  $U_{CB}$ . However, as shown in Figure 4c, the smaller weighted mobility ratio ( $A = U_{CB}/U_{VB}$ ) of the S-doped sample suggests that the magnitude of the bipolar conduction

can be reduced [7,16]. The electron and hole carrier concentrations are shown in Figure 4 and Table 1. The electron concentration increased, while the hole concentration decreased with the S doping, which also reduced the bipolar conduction.

**Table 1.** Band parameters estimated using the two-band model (see Section S1 in Supplementary Materials).

$\text{Cu}_{0.008}\text{Bi}_2\text{Te}_{2.8-x}\text{Se}_{0.2}\text{S}_x$				
Band Parameters		$x = 0$	$x = 0.05$	$x = 0.15$
Conduction Band	CB $E_{def}$ (eV)	17.9	19.0	19.1
	CB $m^*$ (in $m_0$ )	1.07	1.14	1.24
	$U_{CB}$ ( $\text{cm}^2/\text{Vs}$ )	302	254	230
	Electron concentration ( $10^{19} \text{ cm}^{-3}$ )	2.81	4.20	4.72
Valence Band	VB $E_{def}$ (eV)	29.8	25.8	26.5
	VB $m^*$ (in $m_0$ )	1.00	1.00	1.00
	$U_{VB}$ ( $\text{cm}^2/\text{Vs}$ )	117	157	148
	Hole concentration ( $10^{16} \text{ cm}^{-3}$ )	4.71	2.66	2.61
$A (= \frac{U_{CB}}{U_{VB}})$		2.58	1.62	1.55
Bandgap (eV)		0.152	0.156	0.159

Figure 5a shows the  $\kappa_{tot}$  values of the measured samples as functions of the temperature. Despite the increase in the  $\sigma$  of the sample with  $x = 0.05$ , its  $\kappa_{tot}$  was unchanged. The  $\kappa_{tot}$  of the sample with  $x = 0.15$  was smaller than those of the other samples. To understand the change in the thermal transport behavior by S doping, we separated the electronic (electronic thermal conductivity,  $\kappa_{ele}$ ), bipolar ( $\kappa_{bp}$ ), and lattice contributions ( $\kappa_{latt}$ ) from  $\kappa_{tot}$ . The electronic thermal conductivity,  $\kappa_{ele}$ , was estimated using the Wiedemann–Franz law. The calculations of  $\kappa_{bp}$  and  $\kappa_{latt}$  are described in Sections S1 and S2 in the Supplementary Materials, respectively. Figure 5b presents the  $\kappa_{bp}$  calculated using the two-band model based on the fitted parameters listed in Table S1 and shows the reduction in  $\kappa_{bp}$  with S doping. A reduction in  $\kappa_{bp}$  was expected considering the decrease in  $A$  and the increase in the electron concentration in Figure 4a. Thus, the  $\kappa_{bp}$  was reduced by the S doping, which induced the bandgap widening shown in Figure 3a. The experimental  $\kappa_{latt}$  ( $= \kappa - \kappa_{ele} - \kappa_{bp}$ ) values are shown as symbols in Figure 5c, which are well matched with the calculated theoretical  $\kappa_{latt}$  (lines). The theoretical  $\kappa_{latt}$  calculation is presented in Section S2 in the Supplementary Materials [18]. The experimental and theoretical  $\kappa_{latt}$  values decreased with the doping, which implies an additional phonon scattering originated from the doped S. Owing to the effects of the mass and lattice constant differences between the two constituents of the alloy, a large additional contribution from phonon scattering was observed, owing to the large mass and ionic radius differences between S and Te/Se (atomic masses  $M_{\text{Te}} = 127.60 \text{ u}$ ,  $M_{\text{Se}} = 78.96 \text{ u}$ ,  $M_{\text{S}} = 32.06 \text{ u}$ , ionic radii  $r_{\text{Te}} = 221 \text{ pm}$ ,  $r_{\text{Se}} = 198 \text{ pm}$ , and  $r_{\text{S}} = 184 \text{ pm}$ ). Considering the rather large  $\Delta M$  and  $\Delta a$  values, the additional phonon scattering was expected.

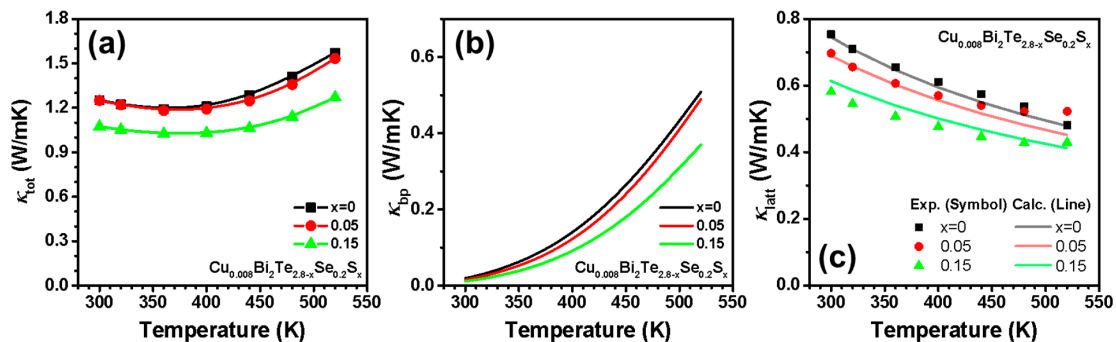


**Figure 5.** (a) Total thermal conductivities,  $\kappa_{tot}$ , (b) bipolar thermal conductivities,  $\kappa_{bp}$ , and (c) lattice thermal conductivities,  $\kappa_{latt}$ , of  $\text{Cu}_{0.008}\text{Bi}_2\text{Te}_{2.8-x}\text{Se}_{0.2}\text{S}_x$  ( $x = 0, 0.05$ , and  $0.15$ ).

The temperature-dependent  $zT$  is shown in Figure 6. The temperature at which the  $zT$  had the maximum value was shifted to a higher temperature and high  $zT$  values of around 0.8 were retained. The lower  $zT$  values of the doped samples at lower temperatures originated from their low power factors (inset of Figure 2b) owing to the large suppression of carrier transport by the S doping. However, the  $zT$  of the sample with  $x = 0.15$  above 400 K was higher than that of the undoped sample, mainly owing to the reductions in  $\kappa_{bp}$  and  $\kappa_{latt}$ , which originated from the S doping.

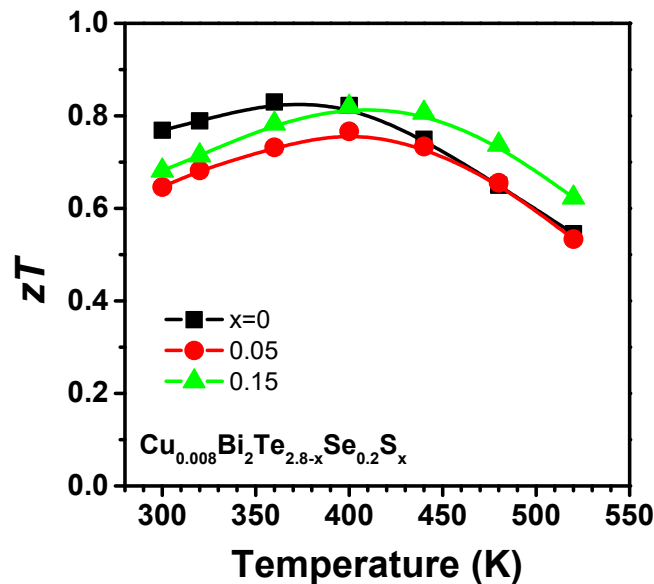


Figure 6.  $zT$  values of  $\text{Cu}_{0.008}\text{Bi}_2\text{Te}_{2.8-x}\text{Se}_{0.2}\text{S}_x$  ( $x = 0, 0.05$ , and  $0.15$ ) as functions of the temperature.

#### 4. Conclusions

In this study, the band modification of  $n$ -type  $\text{Cu}_{0.008}\text{Bi}_2(\text{Te},\text{Se})_3$  alloys by S doping, which could widen the bandgap, was investigated regarding the carrier transport properties and the bipolar thermal conductivity. The bandgap calculated using the Goldsmid–Sharp estimation increased with the S doping. The carrier transport characteristics and thermal conductivity showed the reduction in bipolar conduction. The carrier transport characteristics showed that the weighted mobility ratio was reduced, while the electron carrier concentration was increased. The bipolar thermal conductivity was reduced by the S doping. However, electron mobility was reduced as a detrimental effect of the S doping, which reduced the power factor. The S doping induced additional point-defect phonon scattering and decreased the lattice thermal conductivity. The  $zT$  values at high temperatures were increased by the S doping owing to the simultaneous reductions in bipolar and lattice thermal conductivities.

**Supplementary Materials:** The following are available online at <http://www.mdpi.com/1996-1073/13/2/337/s1>: Table S1: Point defect contributions to the total relaxation rates ( $\tau_{\text{total}}^{-1}$ ) used to model the  $\kappa_{\text{latt}}$  values of the samples.

**Author Contributions:** Conceptualization, W.H.S. and S.Y.K.; Investigation, S.-w.H. and S.-s.C.; Data Curation, Y.O., Y.Y., and Y.K.; Writing–Original Draft Preparation, H.-S.K. and S.-i.K.; Writing–Review & Editing, H.J.P.; Supervision, Project Administration, S.-i.K. All authors have read and agreed to the published version of the manuscript.

**Funding:** This study was supported by Samsung Research Funding & Incubation Center of Samsung Electronics under Project Number SRFC-MA1701-05.

**Conflicts of Interest:** The authors declare no conflict of interest.

## References

1. Bell, L.E. Cooling, heating, generating power, and recovering waste heat with thermoelectric systems. *Science* **2008**, *321*, 1457–1461. [[CrossRef](#)]
2. Scherrer, H.; Scherrer, S. *Thermoelectrics Handbook: Macro to Nano*; Rowe, D.M., Ed.; CRC Press: Boca Raton, FL, USA, 2006; pp. 1–27.
3. Cho, H.-J.; Shin, W.H.; Choo, S.-S.; Kim, J.-I.; Yoo, J.; Kim, S.-I. Synergistic Influence of Cu Intercalation on Electronic and Thermal Properties of *n*-Type  $\text{Cu}_x\text{Bi}_2\text{Te}_{2.7}\text{Se}_{0.3}$  Polycrystalline Alloys. *J. Electron. Mater.* **2019**, *48*, 1951–1957. [[CrossRef](#)]
4. Kim, K.; Kim, G.; Kim, S.I.; Lee, K.H.; Lee, W. Clarification of electronic and thermal transport properties of Pb-, Ag-, and Cu-doped *p*-type  $\text{Bi}_{0.52}\text{Sb}_{1.48}\text{Te}_3$ . *J. Alloys Compd.* **2019**, *772*, 5930602. [[CrossRef](#)]
5. Greenaway, D.L.; Harbeke, G. Band structure of bismuth telluride, bismuth selenide and their respective alloys. *J. Phys. Chem. Solids* **1965**, *26*, 1585–1604. [[CrossRef](#)]
6. Bahk, J.-H.; Shakouri, A. Minority carrier blocking to enhance the thermoelectric figure of merit in narrow-band-gap semiconductors. *Phys. Rev. B* **2016**, *93*, 165209. [[CrossRef](#)]
7. Gibbs, Z.; Kim, H.-S.; Wang, H.; Snyder, C.J. Band gap estimation from temperature dependent Seebeck measurement—Deviations from the  $2e|S|_{\text{max}}T_{\text{max}}$  relation. *Appl. Phys. Lett.* **2015**, *106*, 022112. [[CrossRef](#)]
8. Kim, H.-S.; Lee, K.H.; Yoo, J.; Shin, W.H.; Roh, J.W.; Hwang, J.-Y.; Kim, S.W.; Kim, S.-i. Suppression of bipolar conduction via bandgap engineering for enhanced thermoelectric performance of *p*-type  $\text{Bi}_{0.4}\text{Sb}_{1.6}\text{Te}_3$  alloys. *J. Alloys Compd.* **2018**, *741*, 869–874. [[CrossRef](#)]
9. Liu, W.; Lukas, K.C.; McEnaney, K.; Lee, S.; Zhang, Q.; Opeil, C.P.; Chen, G.; Ren, Z. Studies on the  $\text{Bi}_2\text{Te}_3$ – $\text{Bi}_2\text{Se}_3$ – $\text{Bi}_2\text{S}_3$  system for mid-temperature thermoelectric energy conversion. *Energy Environ. Sci.* **2013**, *6*, 552–560. [[CrossRef](#)]
10. Su, S.-H.; Shu, Y.-T.; Chang, Y.-H.; Chiu, M.-H.; Hsu, C.-L.; Hsu, W.-T.; Chang, W.-H.; He, J.-H.; Li, L.-J. Band Gap-Tunable Molybdenum Sulfide Selenide Monolayer Alloy. *Small* **2014**, *10*, 2589–2594. [[CrossRef](#)] [[PubMed](#)]
11. Kim, J.-I.; Kim, H.-S.; Kim, S.-I. Electrical and thermal transport properties of S- and Te-doped InSe alloys. *J. Phys. D* **2019**, *52*, 295501. [[CrossRef](#)]
12. Li, H.; Han, X.; Pan, D.; Yan, X.; Wang, H.-W.; Wu, C.; Cheng, G.; Zhang, H.; Yang, S.; Li, B.; et al. Bandgap Engineering of InSe Single Crystals Through S Substitution. *Cryst. Growth Des.* **2018**, *18*, 2899–2904. [[CrossRef](#)]
13. Jiang, J.; Chen, L.; Bai, S.; Yao, Q.; Wang, Q. Fabrication and thermoelectric performance of textured *n*-type  $\text{Bi}_2(\text{Te},\text{Se})_3$  by spark plasma sintering. *Mater. Sci. Eng. B* **2015**, *117*, 334–338. [[CrossRef](#)]
14. Liu, W.S.; Zhang, Q.; Lan, Y.; Chen, S.; Yan, X.; Zhang, Q.; Wang, H.; Wang, O.; Chen, G.; Ren, Z. Thermoelectric Property Studies on Cu-Doped *n*-type  $\text{Cu}_x\text{Bi}_2\text{Te}_{2.7}\text{Se}_{0.3}$  Nanocomposites. *Adv. Energy Mater.* **2011**, *1*, 577. [[CrossRef](#)]
15. Lognone, Q.; Gascoin, F. Reactivity, stability and thermoelectric properties of *n*- $\text{Bi}_2\text{Te}_3$  doped with different copper amounts. *J. Alloys Compd.* **2014**, *610*, 1–5. [[CrossRef](#)]
16. Goldsmid, H.J.; Sharp, J.W. Estimation of the thermal band gap of a semiconductor from seebeck measurements. *J. Electron. Mater.* **1999**, *28*, 869–872. [[CrossRef](#)]
17. May, A.F.; Snyder, G.J. *Materials, Preparation, and Characterization in Thermoelectric*; CRC Press: Boca Raton, FL, USA, 2012; pp. 1–18.
18. Callaway, J. Model for lattice thermal conductivity at low temperatures. *Phys. Rev.* **1959**, *113*, 1046–1051. [[CrossRef](#)]

